Glass-Transition and Gas-Transport Characteristics of Polymer Nanocomposites Based on Crosslinked Poly(ethylene oxide)

Anthony C. Comer,[1] Douglass S. Kalika,[1] Victor A. Kusuma,[2] Benny D. Freeman[2]

[1]*Department of Chemical and Materials Engineering, University of Kentucky, Lexington, Kentucky 40506-0046*
[2]*Center for Energy and Environmental Resources, Department of Chemical Engineering, University of Texas, Austin, Texas 78758*

Received 14 August 2009; accepted 8 January 2010
DOI 10.1002/app.32081
Published online 13 April 2010 in Wiley InterScience (www.interscience.wiley.com).

ABSTRACT: The glass-transition and gas-transport properties of rubbery polymer nanocomposites based on crosslinked poly(ethylene oxide) and metal oxide nanoparticles were studied. Nanocomposite samples were prepared by the UV photopolymerization of poly(ethylene glycol) diacrylate ($n \sim 14$) in the presence of magnesium oxide or silica nanoparticles. The thermomechanical properties of the composites were investigated with dynamic mechanical and dielectric spectroscopy methods. The inclusion of nanoparticles in the crosslinked poly(ethylene glycol) diacrylate network led to a systematic increase in rubbery modulus and a modest positive offset (~6°C) in the measured glass-transition temperature for both systems. Bulk density measurements indicated only minimal void volume fraction in the composites, and CO_2 and light gas permeability decreased with particle loading; for example, the CO_2 infinite dilution permeability at 35°C decreased from 106 barrer in the unfilled polymer to 55 barrer in a nanocomposite containing 30 wt % magnesium oxide nanoparticles. The inclusion of toluene diluent in the prepolymerization mixtures produced a limited enhancement in sample permeability, but the sizeable increases in gas transport with particle loading reported for certain other rubbery nanocomposite systems were not realized in the crosslinked poly(ethylene glycol) diacrylate composites. © 2010 Wiley Periodicals, Inc. J Appl Polym Sci 117: 2395–2405, 2010

Key words: glass transition; nanocomposites; membranes

INTRODUCTION

The removal of acid gases such as carbon dioxide from light gas mixtures via membrane separation technology is an area of intense interest because of the relevance of such separations for a range of industrial processes. Recently, a series of rubbery copolymer membranes based on crosslinked poly(ethylene oxide) (XLPEO) has been investigated for use in CO_2/light gas separations.[1,2] The polymers display high CO_2 permeability and favorable CO_2/light gas selectivity because of their rubbery character and the presence of polar ether oxygens in the polymer network that interact preferentially with CO_2.[3] The strategic copolymerization of XLPEO has been used to tailor the free volume and chemical composition of the networks; this led to the establishment of material design rules for the optimization of gas separation performance in these CO_2-selective membranes.[4–8]

The introduction of nanoscale structure in polymers via the inclusion of inorganic nanoparticles provides a range of variables that can be exploited for the enhancement of material properties. In the case of gas separation membranes, recent studies have demonstrated improvements in gas separation performance that can be achieved upon the incorporation of metal oxide nanoparticles into glassy and rubbery polymers, with the presence of the filler leading to changes in both the diffusivity and solubility characteristics of the membranes. For example, the introduction of hydrophobic fumed silica (SiO_2) into glassy, high-free-volume poly(4-methyl-2-pentyne) produces a disruption in polymer chain packing that leads to a subtle, angstrom-level increase in the free volume available for penetrant transport; this results in a systematic increase in the diffusivity with filler loading.[9,10] The enhancement in gas-transport properties is higher in samples containing smaller nanoparticles, which suggests the importance of the surface-to-volume ratio in these

Correspondence to: D. S. Kalika (kalika@engr.uky.edu).
Contract grant sponsor: American Chemical Society Petroleum Research Fund; contract grant number: PRF #45353-AC7 (for support of research activities conducted at the University of Kentucky).
Contract grant sponsor: U.S. Department of Energy; contract grant number: DE-FG02-02ER15362 (for research performed at the University of Texas at Austin).
Contract grant sponsor: U.S. National Science Foundation; contract grant number: CBET-0515425 (for research performed at the University of Texas at Austin).

materials. Similarly, the incorporation of metal oxide nanoparticles into rubbery 1,2-polybutadiene (PB) generates a marked increase in the permeability, which reflects a combination of higher penetrant solubility due to physical adsorption and increased diffusivity.[11,12] The enhancement in diffusivity for the polybutadiene composites is due primarily to the presence of a substantial void volume fraction detected in the solvent-cast samples.

Because of the potential of XLPEO network polymers for use as CO_2-selective membranes and the commercial availability of very small metal-oxide-based nanoparticles, it is of interest to explore possible enhancements in XLPEO gas separation performance due to the incorporation of metal oxide nanoparticles; for example, magnesium oxide (MgO) and SiO_2. When one assesses the influence of nanoparticles on gas transport, it is important to consider the extent to which the particles perturb the surrounding polymer, as changes in the polymer chain mobility affect the size discrimination and the corresponding penetrant diffusivity characteristics of the matrix. In rubbery polymers, segmental mobility is responsible for the creation of transient free-volume elements by which gas diffusion occurs. The glass-transition temperature (T_g) can be used as an indicator of overall segmental mobility, and a number of authors have reported correlations wherein the measured light gas permeability and diffusivity decreased systematically with increasing T_g across a range of rubbery polymers.[13]

The vast amount of particle–polymer surface area created in nanocomposites can have a substantial influence on the segmental mobility of the polymer chains because of both particle–polymer interactions and physical confinement effects; these perturbations to the bulk polymer chain dynamics are often manifested by changes in T_g. Over the last several decades, there have been numerous reports examining the glass-transition characteristics of filled polymers reinforced with materials such as carbon black or SiO_2, and more recently, such systems have been studied within the context of nanoscale phenomena. In filled polymers, the inclusion of inorganic particles often leads to an increase in T_g because of favorable interactions between the particle surface and the polymer chains that restrict chain mobility.[14] Investigators have reported positive offsets in T_g and the emergence of a second (higher) T_g corresponding to the presence of a distinct, constrained population of chain segments in the vicinity of the particle surface.[15–19] For systems that exhibit poor wetting, T_g reductions have also been encountered.[20,21] In certain cases, a direct correlation has been demonstrated between the T_g values measured for bulk composites and the influence of physical confinement on T_g observed for ultrathin polymer films.[22–24]

In this study, we examined the glass-transition and gas-permeability characteristics of a series of rubbery polymer nanocomposites based on crosslinked poly(ethylene glycol) diacrylate (XLPEGDA). Nanocomposite samples were prepared by UV photopolymerization of poly(ethylene glycol) diacrylate (PEGDA) in the presence of various amounts of nominally spherical MgO or SiO_2 nanoparticles. The glass–rubber relaxation characteristics of the resulting polymers were assessed with dynamic mechanical analysis and dielectric spectroscopy. Gas-permeability results are reported for CO_2, CH_4, O_2, and H_2, along with the gas diffusion and solubility coefficients. In addition, the influence of sample preparation in the presence of toluene as a potential particle dispersion aid is reported.

EXPERIMENTAL

Materials

The crosslinker PEGDA (nominal molecular weight = 700 g/mol) and the photoinitiator 1-hydroxyl cyclohexyl phenyl ketone (HCPK) were obtained from Aldrich Chemical Co. (Milwaukee, WI). The molecular weight and polydispersity of the PEGDA were characterized previously; a number-average molecular weight of 743 g/mol was reported, consistent with a monomeric repeat length of $n \approx 14$ (see ref. 4). Spherical MgO nanoparticles (99.2% purity) were obtained from Nanoscale Materials, Inc. (Manhattan, KS). The manufacturer reported an effective density for these particles of 2.4 g/cm^3 and a Brunauer–Emmett–Teller surface area of 600 m^2/g; this corresponded to a nominal particle diameter of approximately 3 nm.[11] SiO_2 nanoparticles (99.5% purity, 10 nm diameter) were obtained from Aldrich, with a reported Brunauer–Emmett–Teller surface area of 590–690 m^2/g and a density of 2.2 g/cm^3. Toluene (high-performance liquid chromatography grade) was purchased from Fisher Scientific (Pittsburgh, PA). All gases were obtained from Airgas Southwest, Inc. (Corpus Christi, TX), with purity of at least 99.9% (except for methane, which had a purity of 99.0%), and were used as received.

Preparation of the nanocomposites

PEGDA, HCPK (0.1 wt % based on PEGDA), and the nanoparticles were magnetically mixed in desired proportions for at least 20 min; they were then sonicated in an ultrasonic water bath for 10 min to eliminate bubbles (model FS60, Fisher Scientific). In cases where toluene was added to aid particle dispersion (i.e., at higher particle loadings), PEGDA, HCPK, and toluene were first magnetically mixed for at least 20 min; then, the nanoparticles

were added and mixed for an additional 20 min before degassing. All of the mixtures were then subjected to planetary mixing for 3 min at 2000 rpm in a Thinky Planetary Mixer model AR-250 (Thinky Corp., Laguna Hills, CA).

Samples were crosslinked via UV photopolymerization with a Spectrolinker XL-1000 crosslinker (Spectronics Corp., Westbury, NY). The mixture was sandwiched between parallel quartz plates with controlled spacing and exposed to 312-nm UV light for 90 s at 3 mW/cm^2, as per the method for XLPEGDA polymerization described previously.[4,25] After crosslinking, the films were stored *in vacuo* at 25°C for at least 24 h before further study. Films prepared with toluene diluent were immediately covered after crosslinking to control the rate of toluene evaporation; after they were initially dried in a fume hood, these samples were held *in vacuo* at room temperature (25°C). The thickness of the resulting nanocomposite films was approximately 1.0 mm for dynamic mechanical specimens and approximately 0.30 mm for samples prepared for dielectric measurement and permeability tests; the precise thickness of each film was determined with a digital micrometer with a precision of ±1 μm.

Film density

Bulk density measurements of the crosslinked nanocomposite films were conducted by hydrostatic weighing at 25°C with a conventional density determination kit (Denver Instrument, Bohemia, NY); *n*-heptane was used as the auxiliary liquid. A minimum of three replicate measurements were completed for each sample tested.

Dynamic mechanical analysis

Dynamic mechanical analysis was performed with a Polymer Laboratories (Amherst, MA) dynamic mechanical thermal analyzer operating in single-cantilever bending geometry. All specimens were dried *in vacuo* at room temperature for at least 24 h before measurement, and the sample mounting procedures were designed to minimize exposure to ambient moisture. Storage modulus (E') and loss tangent (tan δ) were recorded at a heating rate of 1°C/min with test frequencies of 0.1, 1, and 10 Hz. Each measurement was carried out under an inert (N_2) atmosphere.

Broadband dielectric spectroscopy

Dielectric measurements were conducted with a Novocontrol broadband dielectric spectrometer (Hundsangen, Germany). To promote electrical contact during measurement, concentric 33-mm silver electrodes were applied to each sample film with a Veeco thermal evaporation system (Plainview, NY). Samples were subsequently mounted between gold platens and positioned in a Novocontrol Quatro Cryosystem. The dielectric constant (ε') and dielectric loss (ε'') were recorded at a heating rate of 2°C/min with test frequencies ranging from 1 Hz to 2 MHz.

Gas-transport measurements

Pure gas-permeability values for CO_2, CH_4, O_2, and H_2 were determined with a constant-volume/variable-pressure apparatus.[26,27] The gas flux was measured from the steady-state pressure rise in a preevacuated downstream vessel of fixed volume when pure gas was applied on the upstream side at a known high pressure (3 to 15 atm for the studies conducted here); the samples were partially masked with impermeable aluminum tape on the upstream face of each film to accurately define the surface area available for mass transport and to prevent damage to the film during testing. Permeability values were calculated from steady-state flux measurements,[6] whereas the diffusion coefficients were estimated via time-lag measurements of transient gas flux.[27,28] The corresponding gas-solubility coefficients were determined according to the solution-diffusion model (Solubility coefficient = Permeability coefficient/Diffusion coefficient).[29] The permeability values obtained for CH_4, O_2, and H_2 were independent of upstream pressure, whereas CO_2 exhibited plasticization with increasing pressure (see ref. 4). To compare the inherent permeability of the polymers to different gases, the permeability values are reported at infinite dilution (i.e., extrapolated to an upstream pressure, $p \rightarrow 0$), consistent with our previous studies. All experiments were performed at 35°C.

RESULTS AND DISCUSSION

Dynamic mechanical studies

The UV photopolymerization of the PEGDA ($n = 14$) crosslinker in the presence of various loadings of nanoparticles produced three-dimensional nanocomposite networks; this was consistent with the results obtained for the PEGDA-based formulations studied previously.[4] Independent differential scanning calorimetry studies (not shown) indicated that the polymer matrix was fully amorphous, with no evidence of crystallization.

Dynamic mechanical results for the PEGDA/MgO and PEGDA/SiO_2 nanocomposite films are presented in Figures 1 and 2, respectively, with E' and tan δ plotted versus temperature at a frequency of 1 Hz. The 100% XLPEGDA (unfilled) network

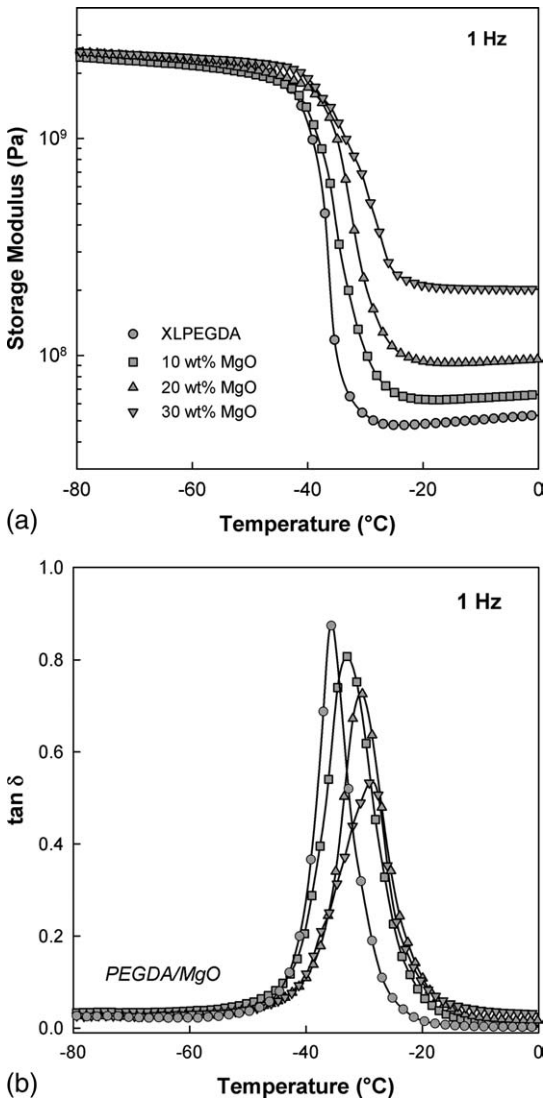

Figure 1 Dynamic mechanical properties versus the temperature for the PEGDA/MgO nanocomposites: (a) E' and (b) tan δ (frequency = 1 Hz; heating rate = 1°C/min).

displayed a glassy modulus of approximately 2.5 GPa and a glass–rubber transition peak temperature (T_α) of −35°C (1 Hz). The rubbery modulus for XLPEGDA (0°C) was approximately 50 MPa. The introduction of MgO nanoparticles had only a minimal influence on the glassy modulus of the network (i.e., <5% enhancement) but produced a strong systematic increase in the rubbery modulus with particle loading because of the larger difference in the inherent moduli of the included and matrix phases in this region.[14,30] The observed increase in the rubbery modulus with loading was accompanied by a systematic decrease in the intensity of tan δ and a shift in the peak position to higher temperatures, that is, a progressive increase in the glass–rubber relaxation temperature. Similar results were obtained for the PEGDA/SiO_2 system (see Fig. 2) but with a slightly greater (∼15%) enhancement in the glassy modulus with loading evident below T_g.

In nanocomposite systems with favorable particle–polymer interactions, increases in T_g with filler loading are often observed, with the magnitude of the increase reflecting a number of interrelated material factors, which include particle size and corresponding interfacial surface area, particle loading and its implications for the average polymer layer thickness surrounding each particle, particle–polymer interaction energy, and relative stiffness of the polymer.[22–24] The measured dynamic mechanical peak temperatures for the PEGDA-based nanocomposites as a function of loading are reported in Figure 3. Across the range of compositions examined, an overall increase in T_α of approximately 6°C was observed. The trend was essentially the same for both systems. Furthermore, there was no evidence to suggest the

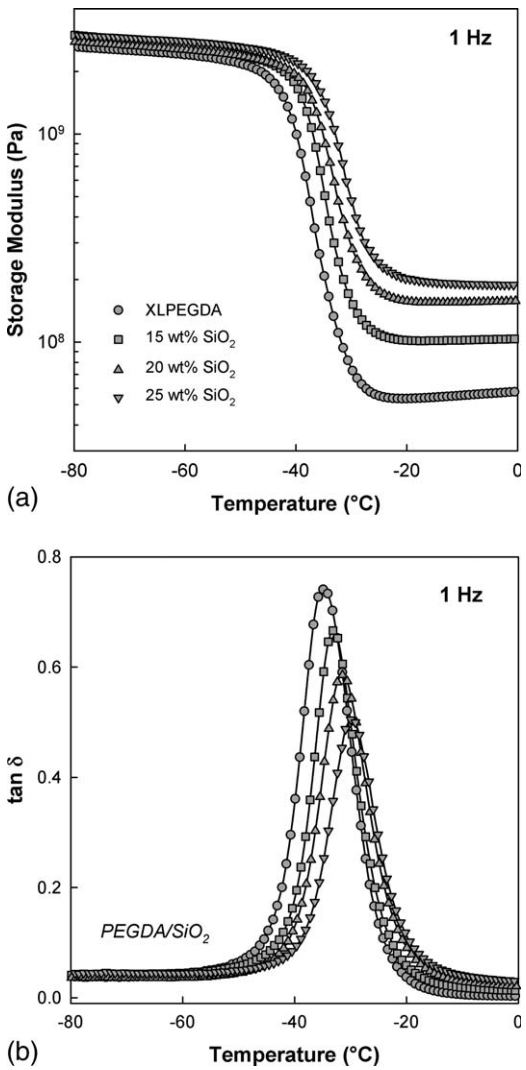

Figure 2 Dynamic mechanical properties versus the temperature for the PEGDA/SiO_2 nanocomposites: (a) E' and (b) tan δ (frequency = 1 Hz; heating rate = 1°C/min).

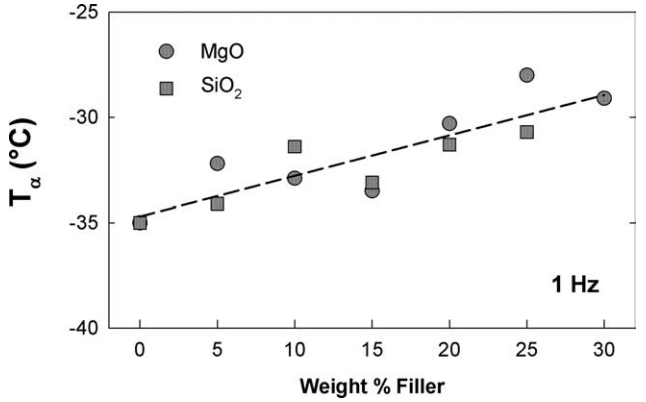

Figure 3 T_α versus the weight percentage of the filler for the XLPEGDA nanocomposites: the glass–rubber transition.

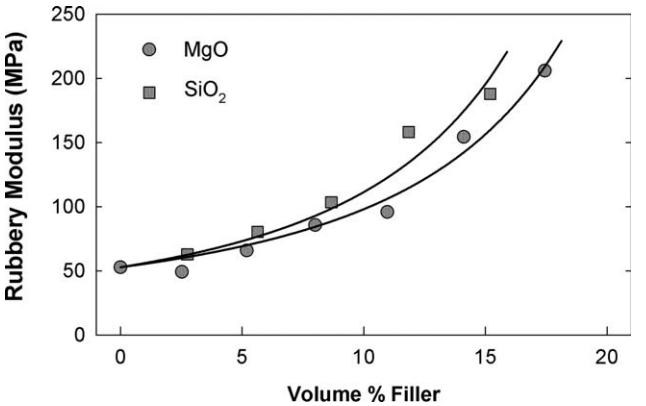

Figure 4 Rubbery modulus (0°C) versus the volume percentage of the filler for the XLPEGDA nanocomposites. The curves are best fits for eq. (2).

emergence of a second, distinct glass-transition process in the composite samples (see Tsagaropoulos and Eisenberg[18]).

The rubbery modulus measured for the various nanocomposites is plotted versus the volume percentage of filler in Figure 4. Here, the volume fraction of the filler (ϕ_F) was determined as follows:

$$\phi_F = \frac{w_F}{w_F + \frac{\rho_F}{\rho_P}(1 - w_F)} \tag{1}$$

where w_F is the weight fraction of the particles, ρ_P is the density of the XLPEGDA polymer matrix (1.183 g/cm^3),[4] and ρ_F is the density of the filler particles. According to the suppliers, ρ_F was 2.4 g/cm^3 for MgO and 2.2 g/cm^3 for SiO_2.

The modulus data presented in Figure 4 could be described with a modified version of the Mooney equation, which, in its original form, describes the viscosity of colloidal suspensions containing rigid spherical particles.[31] In the context of the mechanical modulus, the Mooney equation can be expressed as follows:

$$\ln\left(\frac{E}{E_P}\right) = \frac{k_E \phi_F}{1 - \phi_F/\phi_M} \tag{2}$$

where E is the measured rubbery modulus of the composite, E_P is the modulus of the polymer matrix (50 MPa; see Fig. 1), k_E is the Einstein coefficient, and ϕ_M is the maximum volume fraction of the filler. The value of k_E depends on the quality of the particle–matrix interaction and on the particle distribution (i.e., dispersed vs. agglomerated spheres). For dispersed spheres with no slippage at the interface, $k_E = 2.5$, with higher values obtained in agglomerated systems. Likewise, ϕ_M depends on the packing geometry and the extent of agglomeration, with a maximum value of 0.74 corresponding to an ideal, close-packed arrangement.[14] For the data shown in Figure 4, best-fit curves were obtained with k_E and ϕ_M serving as adjustable parameters. A single value for ϕ_M was obtained for both systems ($\phi_M = 0.45$), with $k_E = 4.8$ (MgO) and 5.8 (SiO_2). The parameter values indicated that the modulus–filler relation was influenced to some degree by particle agglomeration within the XLPEGDA matrix, with the effect being slightly stronger in the case of the PEGDA/SiO_2 composites.[14]

Time–temperature superposition was applied to the dynamic mechanical results to obtain modulus–frequency master curves for the composites at a reference temperature of −40°C.[32] The results are presented in Figure 5 (PEGDA/MgO composites) with E' plotted versus ωa_T, where ω is the applied

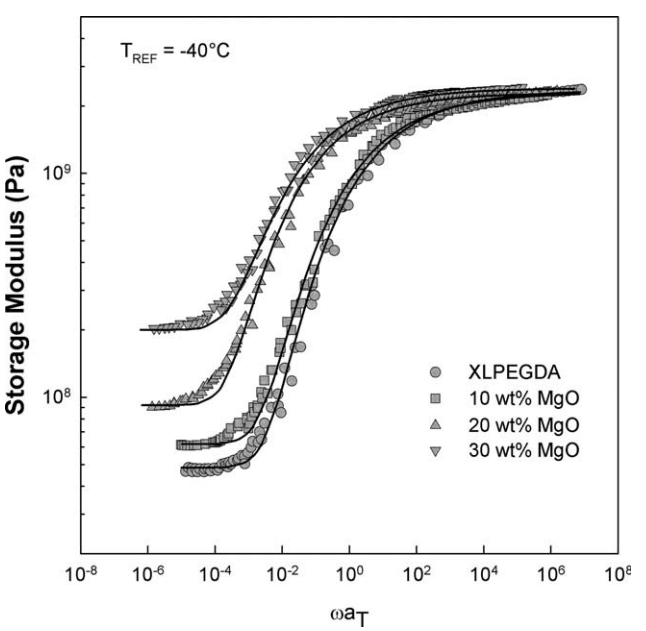

Figure 5 Time–temperature master curves (E' vs ωa_T) for the PEGDA/MgO nanocomposites [reference temperature (T_{REF}) = −40°C]. The solid curves are based on the KWW equation.

test frequency ($\omega = 2\pi f$, where frequency f is expressed in hertz) and a_T is the dimensionless shift factor. The relative positions of the curves along the horizontal axis reflect the effective glass–rubber relaxation time for the samples, with higher MgO loadings leading to longer relaxation times and correspondingly higher T_g values. The time–temperature master curves could be satisfactorily described with the Kohlrausch–Williams–Watts (KWW) stretched-exponential relaxation time distribution function:

$$\alpha(t) = \exp\left[-(t/\tau_0)^{\beta_{KWW}}\right] \quad (3)$$

where τ_0 is the central relaxation time and β_{KWW} is the distribution parameter. β_{KWW} ranges from 0 to 1, with values close to unity corresponding to a narrow, single relaxation time response and lower values reflecting broader transitions influenced by intermolecular coupling, crosslinks, and the presence of crystallinity or other internal constraints. For the data shown in Figure 5, series approximations reported by Williams et al.[33] were used as the basis for the KWW curve fits. A single value for the broadening parameter, $\beta_{KWW} = 0.25 \pm 0.01$, was sufficient to describe the relaxation response for both the PEGDA/MgO and PEGDA/SiO_2 composite series, independent of particle loading. That is, no significant broadening of the XLPEGDA glass–rubber relaxation was encountered with the addition of increasing levels of nanoparticles in these composites.

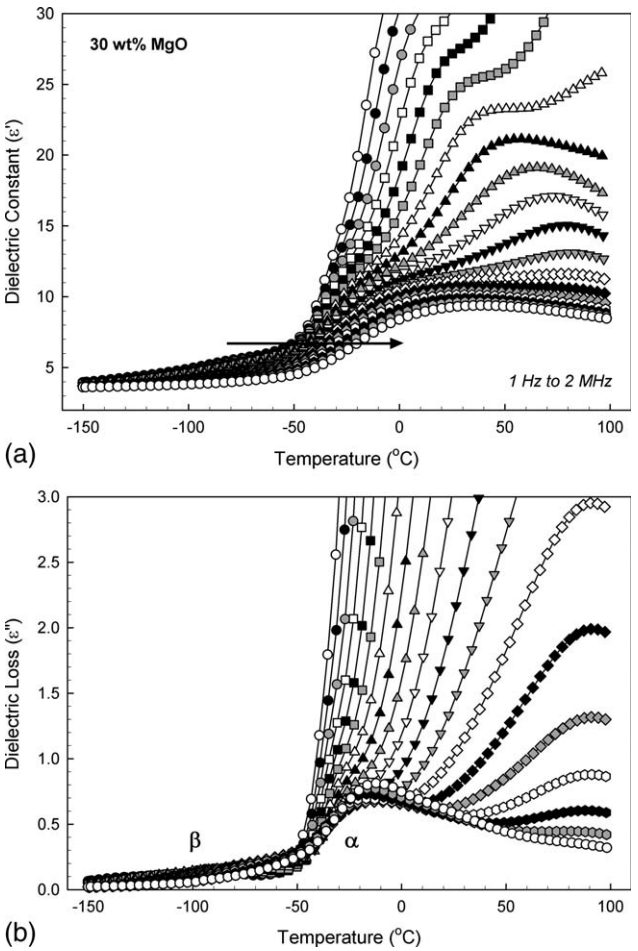

Figure 6 Dielectric properties versus the temperature for the PEGDA/30 wt % MgO nanocomposite: (a) ε' and (b) ε'' (heating rate = 2°C/min; frequency = 1 Hz to 2 MHz). The arrow indicates the direction in which the test frequency increases.

Dielectric spectroscopy studies

Broadband dielectric spectroscopy can serve as a valuable complement to dynamic mechanical measurements for the elucidation of relaxation processes (e.g., the glass transition) in polymer systems. Dielectric spectroscopy relies on the detection of dipolar reorientations along the polymer molecules as the basis for establishing motional transitions, and modern dielectric instruments provide for measurements across an exceptionally wide range of test frequencies. However, in heterogeneous media, the measured dielectric response is complicated by the occurrence of interfacial polarization, which results because of the build-up of charges at the internal boundaries within the material.[34] The contributions to ε' and ε'' from interfacial polarization can be substantial and are most pronounced at low frequencies and temperatures above the glass transition. Although a number of theories have emerged that describe interfacial polarization effects as a function of the electrical properties of the individual constituents and their shape and distribution, the quantitative application of these models is often difficult because of the complexity of the morphology encountered in bulk composite materials.

The dielectric relaxation properties of unfilled XLPEGDA and related copolymers have been studied in detail and were reported in a series of prior publications.[35–37] Representative dielectric results for the nanocomposites (PEGDA + 30 wt % MgO) are given in Figure 6. Examination of ε' versus temperature revealed three polarization processes that appeared as incremental increases in ε': a merged subglass (β) process at low temperatures (~−100°C), the glass–rubber (α) relaxation with an onset temperature of approximately −50°C, and interfacial polarization at temperatures beyond the α transition. Relative maxima in ε'' were observed for each of the three processes; at lower frequencies, the interfacial contribution to ε'' largely obscured the orientational polarization response associated with the glass transition.

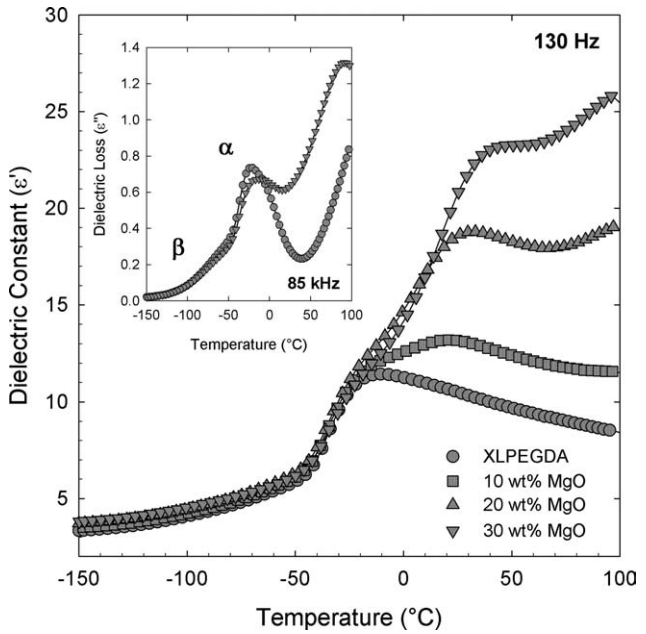

Figure 7 ε′ versus the temperature for the PEGDA/MgO nanocomposites at 130 Hz. The inset shows ε″ versus the temperature for the XLPEGDA/30 wt % MgO composite at 85 kHz.

A comparison of the dielectric results for XLPEGDA and the PEGDA/MgO series of nanocomposites is presented in Figure 7. Plots of ε′ versus temperature at 130 Hz clearly showed the increasing magnitude of the interfacial polarization component with increasing MgO content; note the absence of this contribution for the unfilled XLPEGDA network. At 130 Hz, there was considerable overlap of the glass-transition and interfacial polarization processes, and it was difficult to discern any clear trend in T_g with increasing MgO loading. The inset plot, however, shows the ε″ data at 85 kHz (XLPEGDA + 30 wt % MgO composite), where there was greater separation between the glass–rubber and interfacial processes. Here, the loss peak associated with the glass transition in the composite was offset upward by about 8°C compared to the unfilled polymer network, a result that was in good agreement with the T_g trends obtained from the dynamic mechanical studies.

Nanocomposite density

The measurement of bulk density for polymer nanocomposite samples can often provide insight into the nature of the particle dispersion within the polymer matrix. In particular, negative deviations from volume additivity are often indicative of the presence of voids or defects around the filler particles or the possible formation of agglomerates, features that can have a strong influence on the mechanical and gas-transport properties of the composite.[38] For example, gas-transport studies on rubbery PB nanocomposites reported by Matteucci et al.[11] revealed greater than 10-fold increases in CO_2, CH_4, and N_2 permeability in samples loaded with increasing amounts of MgO nanoparticles (up to 27 vol %). This trend, which ran counter to conventional composite models that predict a reduction in permeability with the incorporation of impermeable filler, was found to correlate with the presence of a substantial void volume fraction in the PB/MgO composites, as indicated by density measurements. Bulk density values for the composites displayed a strong negative deviation relative to predictions on the basis of simple volume additivity, with the apparent void volume estimated to be as high as approximately 50%.

Density measurements for the PEGDA/MgO and PEGDA/SiO_2 nanocomposites are reported as a function of particle loading in Figure 8; each

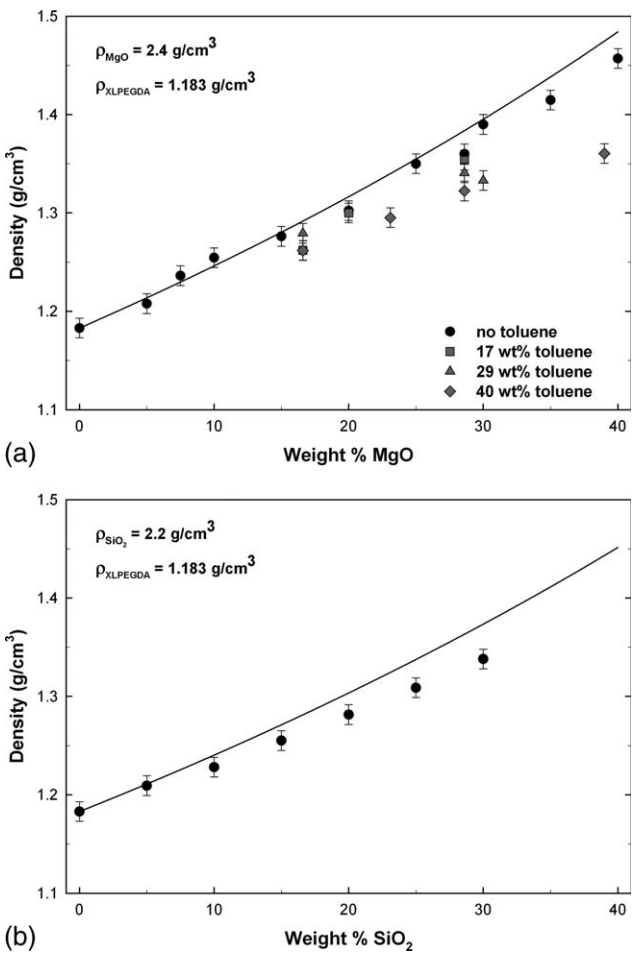

Figure 8 Density (ρ) versus the weight percentage of the filler for the XLPEGDA nanocomposites: (a) PEGDA/MgO and (b) PEGDA/SiO_2. The solid curves correspond to the volume additivity prediction per eq. (4).

plot includes the prediction of the composite density based strictly on volume additivity (ρ_{ADD}):

$$\rho_{ADD} = \rho_F \phi_F + \rho_P \phi_P \quad (4)$$

where ϕ_P is the polymer volume fraction, ρ_F is 2.4 g/cm^3 for MgO and 2.2 g/cm^3 for SiO_2, and ρ_P is 1.183 g/cm^3, as mentioned previously. For the PEGDA/MgO composites synthesized without any added diluent, the measured density closely followed the volume additivity model for loadings up to 30 wt % MgO; this suggested relatively little void volume formation during the preparation of these materials. In the case of the PEGDA/SiO_2 composites, a small negative deviation from volume additivity was observed at higher loadings. The estimated void volume fractions ranged from 0.011 (10 wt % SiO_2) to 0.026 (30 wt % SiO_2).

Additional studies were completed on PEGDA/MgO nanocomposites crosslinked in the presence of toluene, which was added to possibly aid in the dispersion of the nanoparticles before UV exposure.[11] The addition of toluene to the prepolymerization mixture had the potential to alter not only the distribution of nanoparticles but also the properties of the surrounding XLPEGDA matrix. Photopolymerization in the presence of diluent can lead to intramolecular cyclization or loop formation in the polymer network and a corresponding decrease in the effective crosslink density.[39,40] In a separate publication, the influence of toluene on the characteristics of XLPEGDA networks was reported in detail:[41] the photopolymerization of PEGDA crosslinker in the presence of increasing amounts of toluene led to a systematic reduction in the rubbery modulus of the networks because of the formation of loops (i.e., wasted crosslinks), and this was accompanied by a modest decrease in bulk density (ρ_P = 1.171 g/cm^3 for samples prepared with 40 wt % toluene). Density values for the PEGDA/MgO nanocomposites prepared with various levels of toluene are included in Figure 8(a), with toluene content expressed relative to the amount of PEGDA crosslinker in the prepolymerization mixture. For all of the samples, a negative deviation in bulk density was observed relative to nanocomposites prepared under neat conditions. The observed deviation was considerably larger than the density decrease encountered for unfilled XLPEGDA prepared with toluene and may reflect a change in the underlying composite morphology; this could have possibly led to an increase in particle agglomeration and/or greater void volume within the material. The implications of this result with respect to gas permeability in the samples are discussed below.

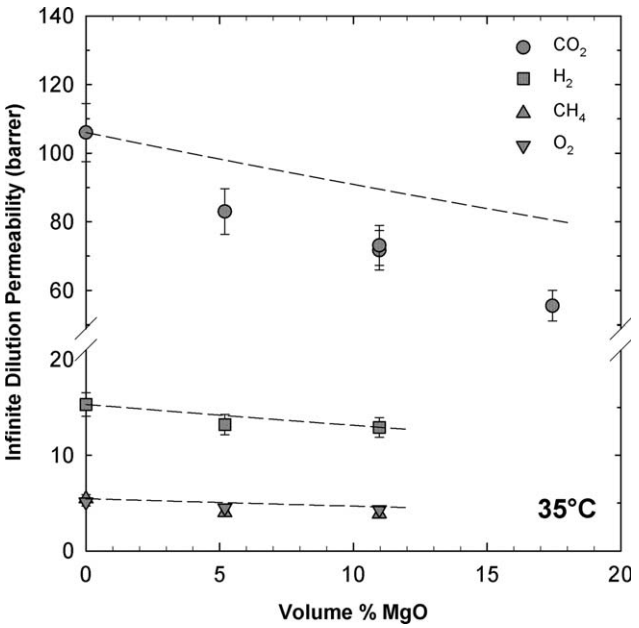

Figure 9 Infinite dilution permeability versus the volume percentage of the filler for the PEGDA/MgO nanocomposites at 35°C [1 barrer = 10^{-10} cm^3 (STP) cm/cm^{2}s cmHg = 7.5 × 10^{-18} m^3 (STP) m/m^{2}s Pa]. The dashed lines correspond to the Maxwell model [eq. (5)].

Gas transport

The remarkable increases in gas permeability observed by Matteucci and coworkers[11,12] for nanoparticle composites based on rubbery PB suggested that similar enhancements could potentially be achieved in CO_2-selective XLPEGDA membrane networks. The inclusion of MgO is of particular interest, as the nanoparticles are basic in character and have the capacity to adsorb CO_2. In the case of the PB/MgO composites, reversible penetrant sorption by the nanoparticles was a significant factor in determining gas-transport characteristics, both in terms of the gas-solubility behavior of the materials and their resultant permeability.

Permeability measurements for the PEGDA/MgO nanocomposites were conducted for CO_2, CH_4, O_2, and H_2 at 35°C and pressures ranging from 3 to 15 atm. The values were extrapolated to an upstream pressure equal to 0, with the reported quantity corresponding to the penetrant permeability at infinite dilution. Although the measured permeabilities for CH_4, O_2, and H_2 were independent of upstream pressure, CO_2 permeability for the various samples at 15 atm was approximately 20–30% higher than the infinite dilution permeability. The results for the XLPEGDA composites as a function of MgO loading are presented in Figure 9. For all gases tested, a systematic decrease in permeability was observed with increasing MgO content, accompanied by a small reduction in CO_2/light gas selectivity. The trend of

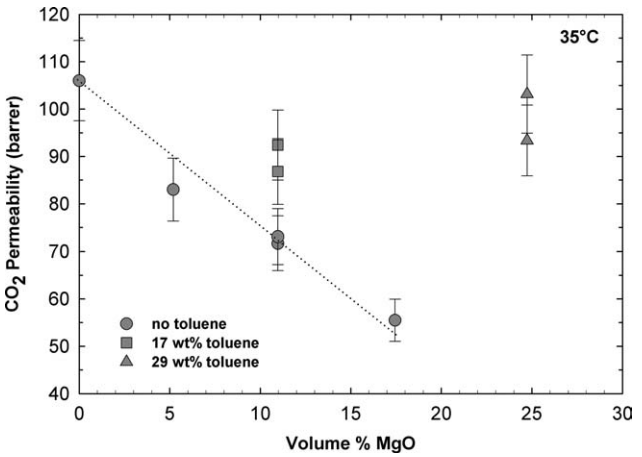

Figure 10 CO_2 permeability at infinite dilution versus the volume percentage of the filler for the PEGDA/MgO nanocomposites at 35°C. The dotted line is a guide for the eye.

the data followed models that describe molecular transport through a polymer matrix containing impermeable spherical filler particles, that is, Maxwell's equation:[42,43]

$$\frac{P_C}{P_P} = \frac{(1-\phi_F)}{\left(1+\frac{\phi_F}{2}\right)} \tag{5}$$

where P_C is the permeability of the composite and P_P is the permeability of the pure polymer network. The results for CH_4, O_2, and H_2 showed good agreement with the Maxwell model (see Fig. 9) and were consistent with data reported by Patel et al.[44,45] for PEGDA crosslinked in the presence of modified fumed SiO_2. The results for CO_2 permeability in the PEGDA/MgO composites were positioned below the Maxwell prediction; this indicated a drop in CO_2 transport with MgO loading that exceeded the anticipated reduction based strictly on the Maxwell expression.

An additional consideration in characterizing the permeability of the PEGDA/MgO composites was the potential influence of the toluene diluent present during the sample preparation process. As noted previously, the inclusion of toluene in the prepolymerization mixture resulted in a reduction in the bulk density of the composites as compared to samples prepared under neat conditions. This led to an increase in the infinite dilution permeability of these samples, as demonstrated for CO_2 in Figure 10. Those composites prepared in the presence of toluene showed markedly higher CO_2 permeability at higher loadings of MgO (i.e., 20 and 40 wt %). However, for all of the composite samples, the permeability remained below the value obtained for the unfilled XLPEGDA network.

Estimates of the gas diffusion coefficients from the transient flux measurements are given in Figure 11 for CO_2, CH_4, and O_2 (the upstream pressure was 4.4 atm). In the case of H_2, the time lag obtained for these samples was too short to establish reliable values. The diffusion coefficients decreased with increasing MgO loading; at 30 wt % (~17.5 vol %) MgO, the CO_2 diffusion coefficient was approximately one order of magnitude below that in neat XLPEGDA. This reduction in diffusivity was likely caused by the presence of the impermeable particles (without any significant increase in the void volume fraction), which increased the tortuosity of the diffusion path. Another factor was the reduction in chain mobility of the polymer matrix with particle loading, as indicated by the increasing glass–rubber transition temperature (cf. Fig. 1). As the chain mobility decreased, the diffusion coefficients could decrease as well; previous studies have demonstrated the importance of polymer chain mobility in determining the gas diffusion characteristics of XLPEO networks.[6,7]

The solubility coefficients were estimated from the permeability and diffusivity values determined at an upstream pressure of 4.4 atm (Solubility coefficient = Permeability coefficient/Diffusion coefficient); these results are presented in Figure 12. A significant increase in CO_2 solubility was observed with increasing MgO loading in a manner consistent with the rubbery PB/MgO composites described by Matteucci et al.[11] In the latter case, the increased CO_2 solubility was attributed to strong gas adsorption by

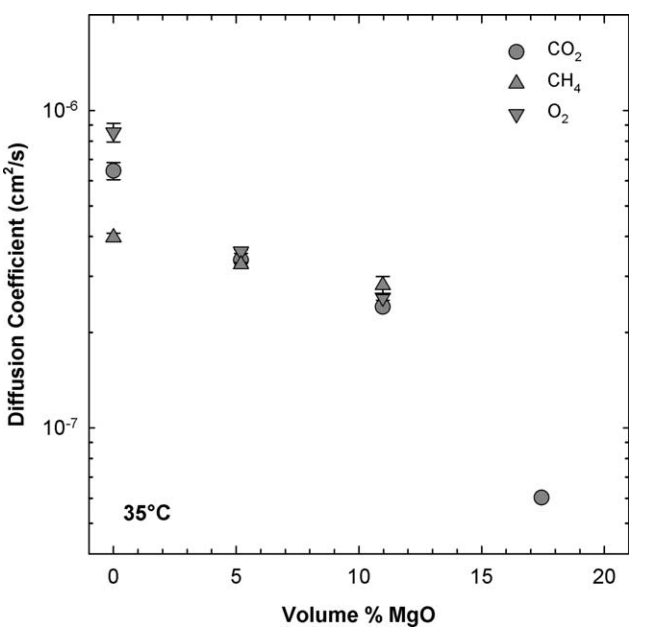

Figure 11 Diffusion coefficient at an upstream pressure of approximately 4.4 atm versus the volume percentage of the filler for the PEGDA/MgO nanocomposites at 35°C as estimated from transient transport measurements.

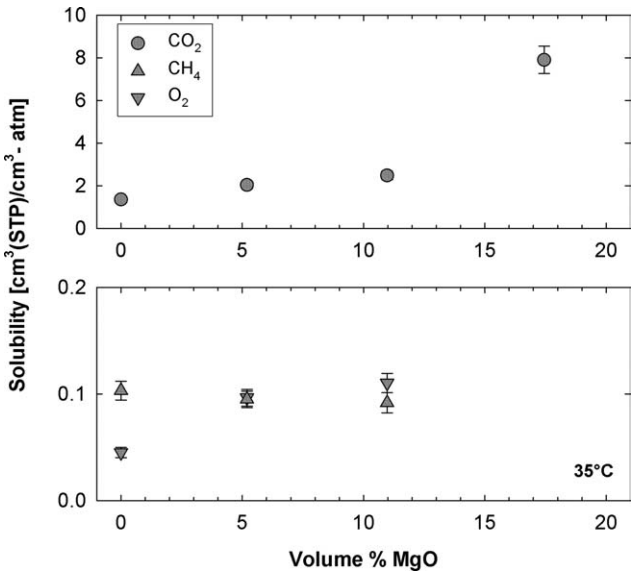

Figure 12 Solubility coefficient at an upstream pressure of approximately 4.4 atm versus the volume percentage of the filler for the PEGDA/MgO nanocomposites at 35°C (solubility coefficient = permeability coefficient/diffusion coefficient).

the MgO nanoparticles. However, the marked increase in void volume fraction observed in the PB/MgO system was not apparent in the *in situ* polymerized PEGDA/MgO composites studied here. Thus, the potential benefits obtained from reversible CO_2 sorption by the nanoparticles were offset by the decreasing overall gas diffusivity, which accounted for the lack of any significant enhancement in the permeability for the PEGDA/MgO system.

CONCLUSIONS

The glass-transition and gas-transport characteristics of a series of polymer nanoparticle composites based on XLPEO were investigated. UV photopolymerization of the PEGDA crosslinker in the presence of MgO or SiO_2 nanoparticles led to the formation of rubbery, amorphous nanocomposite networks. The bulk density values for the nanocomposites were close to volume additivity predictions, with only a minimal void volume fraction indicated at higher particle loadings. The introduction of the nanoparticles in the XLPEGDA network led to a modest increase in T_g for both systems, as measured by dynamic mechanical and dielectric methods (T_g increased by as much as 6°C), but the glass–rubber relaxation breadth remained essentially unchanged with particle loading. The relationship between the rubbery modulus and filler content was described by the Mooney equation, with the resulting parameters suggesting some degree of particle agglomeration within the matrix. Gas-permeability measurements on the PEGDA/MgO series of samples indicated a decrease in infinite dilution permeability with increasing particle loading; this stood in contrast to prior results reported for rubbery PB/MgO composites. The decrease in permeability was attributable to reduced penetrant diffusivity in the composites, which offset enhancements in the (CO_2) gas solubility, resulting from nanoparticle adsorption. PEGDA/MgO nanocomposites prepared in the presence of toluene displayed somewhat higher permeability values compared to the neat formulations, with the data correlating with reduced bulk density and potentially greater void volume in the material.

The authors are pleased to acknowledge the contributions of Sumod Kalakkunnath, Michael Danquah, and Scott Matteucci to the early stages of this work.

References

1. Lin, H.; Van Wagner, E.; Freeman, B. D.; Toy, L. G.; Gupta, R. P. Science 2006, 311, 639.
2. Lin, H.; Van Wagner, E.; Raharjo, R.; Freeman, B. D.; Roman, I. Adv Mater 2006, 18, 39.
3. Lin, H.; Freeman, B. D. J Mol Struct 2005, 739, 57.
4. Lin, H.; Kai, T.; Freeman, B. D.; Kalakkunnath, S.; Kalika, D. S. Macromolecules 2005, 38, 8381.
5. Lin, H.; Van Wagner, E.; Swinnea, J. S.; Freeman, B. D.; Pas, S. J.; Hill, A. J.; Kalakkunnath, S.; Kalika, D. S. J Membr Sci 2006, 276, 145.
6. Kusuma, V. A.; Freeman, B. D.; Borns, M. A.; Kalika, D. S. J Membr Sci 2009, 327, 195.
7. Kusuma, V. A.; Matteucci, S.; Freeman, B. D.; Danquah, M. K.; Kalika, D. S. J Membr Sci 2009, 341, 84.
8. Richards, J. J.; Danquah, M. K.; Kalakkunnath, S.; Kalika, D. S.; Kusuma, V. A.; Matteucci, S. T.; Freeman, B. D. Chem Eng Sci 2009, 64, 4707.
9. Merkel, T. C.; Freeman, B. D.; Spontak, R. J.; He, Z.; Pinnau, I.; Meakin, P.; Hill, A. J. Science 2002, 296, 519.
10. Merkel, T. C.; Freeman, B. D.; Spontak, R. J.; He, Z.; Pinnau, I.; Meakin, P.; Hill, A. J. Chem Mater 2003, 15, 109.
11. Matteucci, S.; Raharjo, R. D.; Kusuma, V. A.; Swinnea, S.; Freeman, B. D. Macromolecules 2008, 41, 2144.
12. Matteucci, S.; Kusuma, V. A.; Swinnea, S.; Freeman, B. D. Polymer 2008, 49, 757.
13. Matteucci, S.; Yampolskii, Y.; Freeman, B. D.; Pinnau, I. In Materials Science of Membranes for Gas and Vapor Separation; Yampolskii, Y.; Pinnau, I.; Freeman, B. D., Eds.; Wiley: New York, 2006; p 1.
14. Nielsen, L. E.; Landel, R. F. Mechanical Properties of Polymers and Composites, 2nd ed.; Marcel Dekker: New York, 1994.
15. Yim, A.; Chahal, R. S.; St. Pierre, L. E. J Colloid Interface Sci 1973, 43, 583.
16. Reid, C. G.; Greenberg, A. R. J Appl Polym Sci 1990, 39, 995.
17. Tsagaropoulos, G.; Eisenberg, A. Macromolecules 1995, 28, 396.
18. Tsagaropoulos, G.; Eisenberg, A. Macromolecules 1995, 28, 6067.
19. Arrighi, V.; McEwen, I. J.; Qian, H.; Prieto, M. B. S. Polymer 2003, 44, 6259.
20. Ash, B. J.; Siegel, R. W.; Schadler, L. S. J Polym Sci Part B: Polym Phys 2004, 42, 4371.
21. Bansal, A.; Yang, H.; Li, C.; Benicewicz, B. C.; Kumar, S. K.; Schadler, L. S. J Polym Sci Part B: Polym Phys 2006, 44, 2944.

22. Bansal, A.; Yang, H.; Li, C.; Cho, K.; Benicewicz, B. C.; Kumar, S. K.; Schadler, L. S. Nat Mater 2005, 4, 693.
23. Rittigstein, P.; Torkelson, J. M. J Polym Sci Part B: Polym Phys 2006, 44, 2935.
24. Rittigstein, P.; Priestley, R. D.; Broadbelt, L. J.; Torkelson, J. M. Nat Mater 2007, 6, 278.
25. Lin, H. Ph.D. Thesis; University of Texas at Austin, 2005.
26. Bondar, V. I.; Freeman, B. D.; Pinnau, I. J Polym Sci Part B: Polym Phys 2000, 38, 2051.
27. Lin, H.; Freeman, B. D. In Springer Handbook of Materials Measurement Methods; Czichos, H.; Saito, T.; Smith, L. E., Eds.; Springer: Berlin, 2006; p 371.
28. Daynes, H. A. Proc R Soc London Ser A 1920, 97, 286.
29. Wijmans, J. G.; Baker, R. W. J Membr Sci 1995, 107, 1.
30. Schwarzl, F. R.; Bree, H. W.; Nederveen, C. J.; Schwippert, G. A.; Struik, L. C. E.; Van der Wal, C. W. Rheol Acta 1966, 5, 270.
31. Mooney, M. J Colloid Sci 1951, 6, 162.
32. Ferry, J. D. Viscoelastic Properties of Polymers, 3rd ed.; Wiley: New York, 1980.
33. Williams, G.; Watts, D. C.; Dev, S. B.; North, A. M. Trans Faraday Soc 1971, 67, 1323.
34. Steeman, P. A. M.; van Turnhout, J. In Broadband Dielectric Spectroscopy; Kremer, F.; Schonhals, A., Eds.; Springer-Verlag: Berlin, 2003; p 495.
35. Kalakkunnath, S.; Kalika, D. S.; Lin, H.; Raharjo, R. D.; Freeman, B. D. Polymer 2007, 48, 579.
36. Kalakkunnath, S.; Kalika, D. S.; Lin, H.; Raharjo, R. D.; Freeman, B. D. Macromolecules 2007, 40, 2773.
37. Borns, M. A.; Kalakkunnath, S.; Kalika, D. S.; Kusuma, V. A.; Freeman, B. D. Polymer 2007, 48, 7316.
38. Takahashi, S.; Paul, D. R. Polymer 2006, 47, 7519.
39. Okay, O.; Kurz, M.; Lutz, K.; Funke, W. Macromolecules 1995, 28, 2728.
40. Kizilay, M.; Okay, O. Macromolecules 2003, 36, 6856.
41. Kusuma, V. A.; Freeman, B. D.; Smith, S. L.; Heilman, A. L.; Kalika, D. S. J Membr Sci, in press.
42. Barrer, R. M. In Diffusion in Polymers; Crank, J.; Park, G. S., Eds.; Academic: New York, 1968; p 165.
43. Maxwell, C. Treatise on Electricity and Magnetism; Oxford University Press: London, 1873.
44. Patel, N. P.; Miller, A. C.; Spontak, R. J. Adv Mater 2003, 15, 729.
45. Patel, N. P.; Miller, A. C.; Spontak, R. J. Adv Funct Mater 2004, 14, 699.